Exploring Operability and Design Characteristics of a Small-Scale Methane/Oxygen Jet-in-Crossflow Rotating Detonation Engine

Aref Abdala[*], Gabriel Shamam[*], Celeste Ozimek-Newman[*], Daniel Sherlock[*], Kathryn Daniel[†], Emil Alunno[*], Erik Solberg[†], Dominic Diatzikis[†], Taha Rezzag[‡]

Propulsion & Energy Research Laboratory.
University of Central Florida, Orlando, FL, 32816, USA

Rotating Detonation Engines (RDEs) are a technology driven by continuous propagation of detonation waves in an annular combustion chamber. RDEs have a wide variety of applications such as, combustors, turbines, aircraft and rocket propulsion devices. Efforts to realize pressure gain with the continuous detonation cycle continue with various forms offering marginal improvements in performance. In progressing the Pressure Gain Combustion (PGC) technology toward field readiness, engine architecture is adapted such that efficiency gains can be maximized while maintaining mechanical simplicity. This study examines a design for a small-scale methane-oxygen jet-in-crossflow RDE with a gaseous propellant scheme. It describes design choices for chamber geometry, injector, manufacturability, and nozzle sizing. Initial calculations were made to determine geometric constraints and were further validated using an analytical model. The analytical model displays wave propagation characteristics and quantity of cells and with different mass flow rates at an equivalence ratio.

I. Introduction

Enhancing the performance of Rotating Detonation Engines (RDEs) has been at the forefront of innovation these past decades. This is because unlike conventional Brayton Cycle engines, RDEs employ a continuous volume combustion process to achieve Pressure Gain Combustion (PGC). The utilization of concepts like the Humphrey Cycle and Fickett-Jacobs cycle has demonstrated superior combustion efficiency compared to traditional cycles [1–7]. Recently, there has been a large increase of interest in Small-Scale Rotating Detonation Rocket Engines (RDREs) [1–7]. The purpose of the work presented is to bridge the gaps of knowledge within the community. There has recently been an increased use of methane for RDE's for experimental analysis. Using the framework provided by Bykovskii's constraints [8] and a mathematical model for small-scale RDRE's, this undergraduate student group embarked on a mission to contribute to the Small-Scale RDRE by designing a Small-Scale Methane/Oxygen Jet-in-Crossflow RDRE.

* Undergraduate Research Assistant, Propulsion Energy & Research Lab, AIAA Student Member.
† Undergraduate Research Assistant, Mechanical and Aerospace Engineering, AIAA Student Member.
‡ Postdoctoral Scientist, Mechanical and Aerospace Engineering, AIAA Professional Member.

II. Design Considerations

A. Chamber Geometry

The combustion chamber is an annulus shape with an outer body that constricts the detonation wave into a rotating path with a center body at the center as shown in the RDRE cross section depicted in Figure 1. The dimensions of the geometry are proportional to the detonation cell width and the desired frequency of detonation; Bykovskii et al's derived sizing constraints heavily influenced the dimensions of the RDRE chamber however some dimensions, such as the channel gap, vary slightly larger than Bykovskii's constraints [8].

Table 1 shows a list of RDRE annulus dimensions, equation used, and the chosen value. The detonation cell width, or cell size is the parameter dependent on the type and ratio of the propellant used as well as the initial pressure inside of the chamber. Figure 2 and figure 3 show a correlation between equivalence ratio and initial chamber pressure that was used to determine a targeted cell size [9]. A smaller cell size is preferred because it will achieve a more stable detonation since there are additional detonation cells that exist in the small channel gap of the chamber. Thus, for this small scale RDRE, a propellant and chamber pressure were chosen to minimize the detonation cells size and the channel gap dimension was chosen that is slightly larger than Bykovskii's constraints.

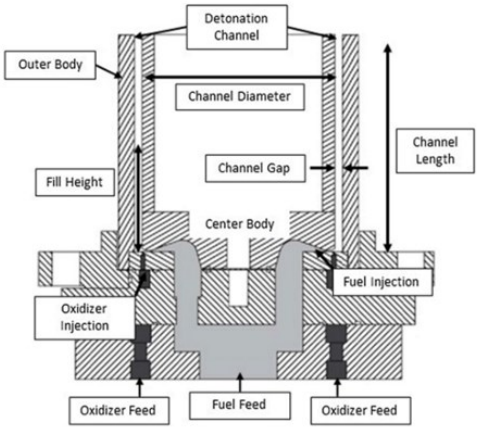

Fig. 1 Typical Cross Section of an RDRE [15]

Parameter	Bykovskii Derived Constraints	Value
Cell Size	λ = Derived	0.35 mm
Critical Length	$C_L = (12 \pm 5)\lambda$	8.5 mm
Channel Gap	$\Delta = 0.2C_L$	2 mm
Channel Length	$l = (3 \pm 1)h$	34 mm
Channel Diameter	$\frac{Wave\ Velocity}{\pi * Frequency}$	36 mm

Table 1 RDRE Chamber Dimensions

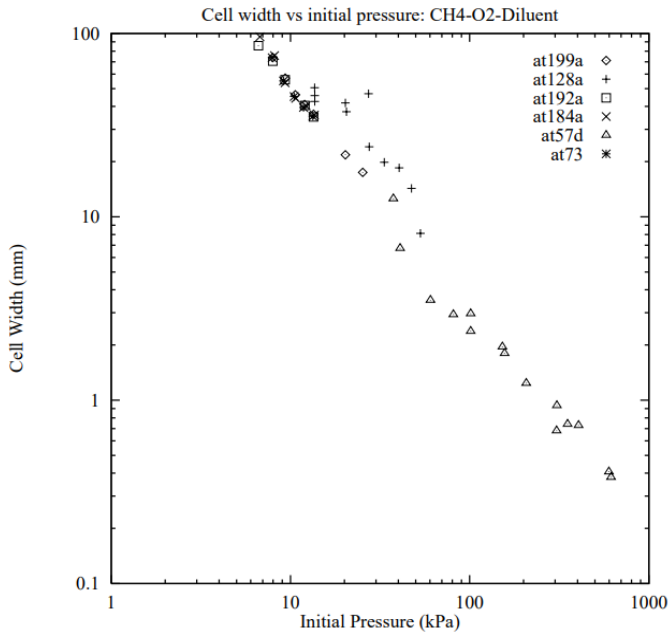

Figure 2 Cell Width and Initial Pressure

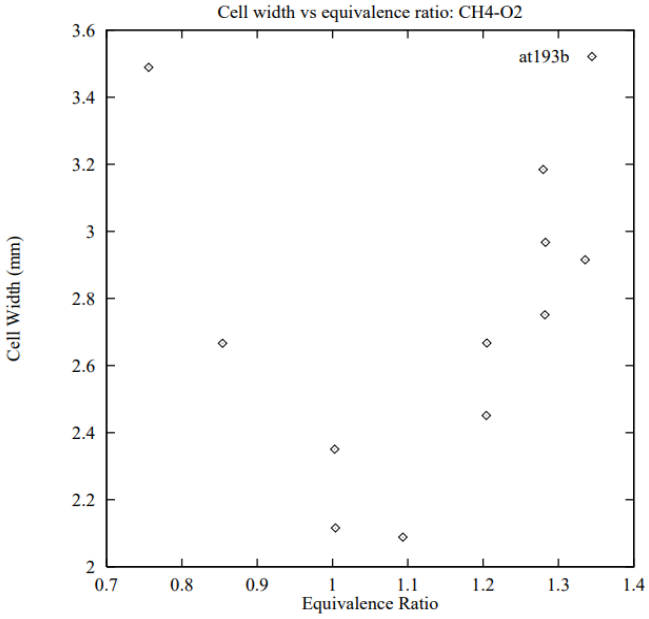

Fig. 3 Cell Width and Equivalence Ratio [9]

The outer body of the combustion chamber consists of multiple interfaces for the pre-detonator and data acquisition (DAQ) sensors that provide pressure and temperature data from capillary tube attenuated pressure (CTAP) transducers and thermocouples, respectively. CTAPs are used to analyze changes chamber pressure that can be used to determine if detonation occurred and its location. The thermocouples will provide temperature data throughout the duration of the engines operation which can be used to determine the outer body's heat flux using the temperature gradients between the detonation temperature and outer body. **Fig.** 4 shows all the interfaces connected to the outer body.

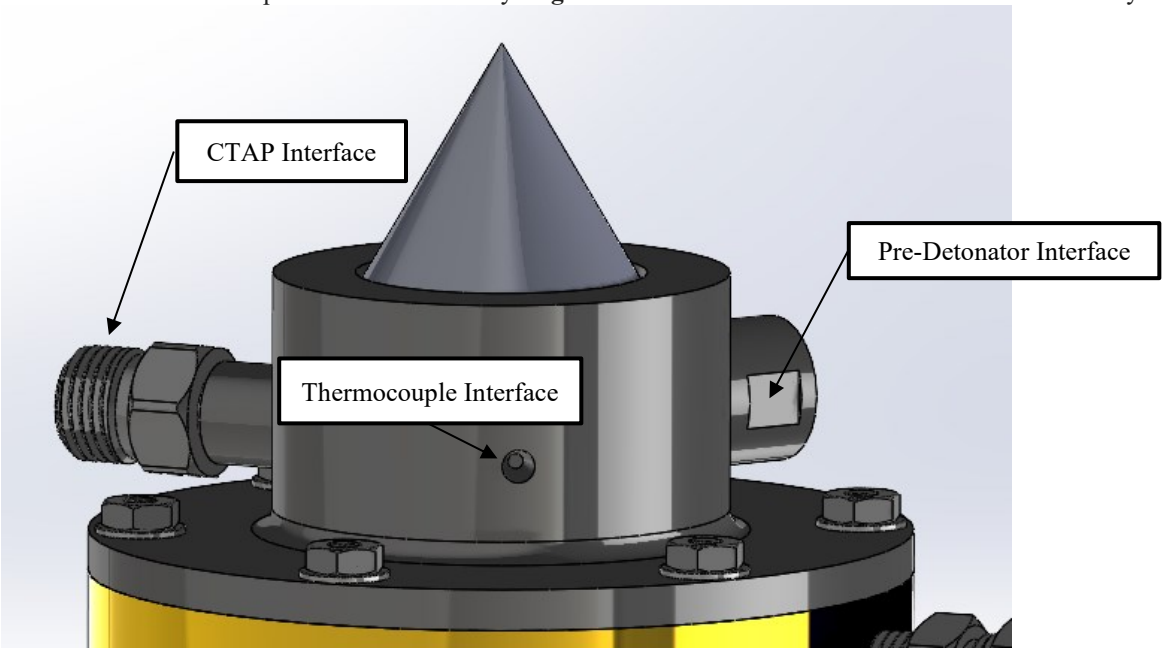

Fig. 4 Outer Body Interfaces

B. RDRE Exit Geometry

Two exit geometries were chosen for the design and testing of this RDRE. Both exit geometries include an aerospike profile. Due to the annular shape of the combustion chamber, there is a region at the exit of the chamber where the flow recirculates back into the inner body which causes an unwanted force acting into RDRE. This unwanted force is often called "negative thrust" due to the kinetic energy loss from the redirected flow. A nozzle with an aerospike geometry fills the void where the flow recirculates and allows all the flow to expand which in return will increase the efficiency of the engine.

Each exit geometry has a unique profile beginning at the exit of the chamber. One geometry has a converging-diverging profile while the other does not. As found by Dechert, Joseph R in his development of a small scale RDRE, having an exit geometry that chokes the flow allows for better reliability in achieving detonation with lower mass flow rates inside the chamber due to the increase in chamber pressure and decrease in flow velocity pre ignition. The main focus of the nozzle will be to improve the reliability of detonation, so the only value calculated for the exit geometry is the area ratios. Many RDREs including the ones developed by Dechert, Joseph R et al and Goto, Keisuke et al found that the lower exit ratio the better the performance and detonation reliability[10,11]. A_t is the area of the throat gap of the choked section of the nozzle and A_c is the area of the channel gap. The diameter of the channel gap, according to Table 1 in the Chamber Geometry section, is equal to 2 mm and with an exit area ratio of 0.26, the diameter of the throat gap is equal to 0.523 mm. This throat gap diameter leads to the throat diameter of the converging-

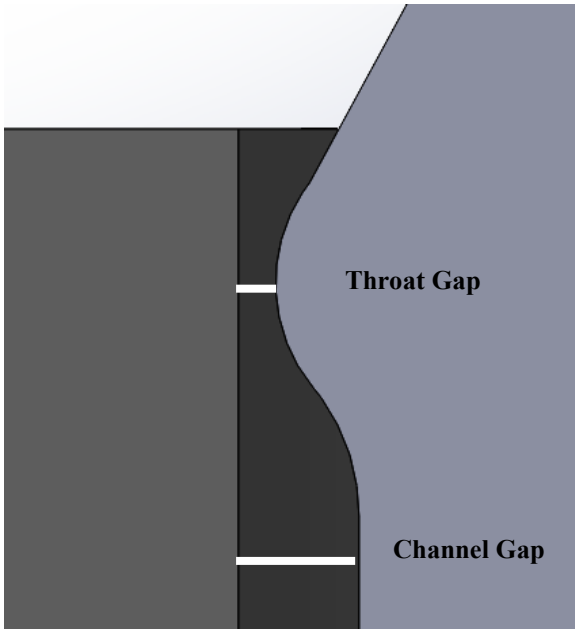

Figure 5 Cross Section of Converging-Diverging Profile

diverging profile of the exit geometry. The throat diameter is equal to 34.95 mm. In the second geometry there is no throat, and the channel gap remains the same all the way through the detonation channel. This yields an exit ratio of 1, since the throat gap diameter is equal to the channel gap diameter.

$$\varepsilon = \frac{A_t}{A_c} = \frac{d_t}{d_c} \tag{1}$$

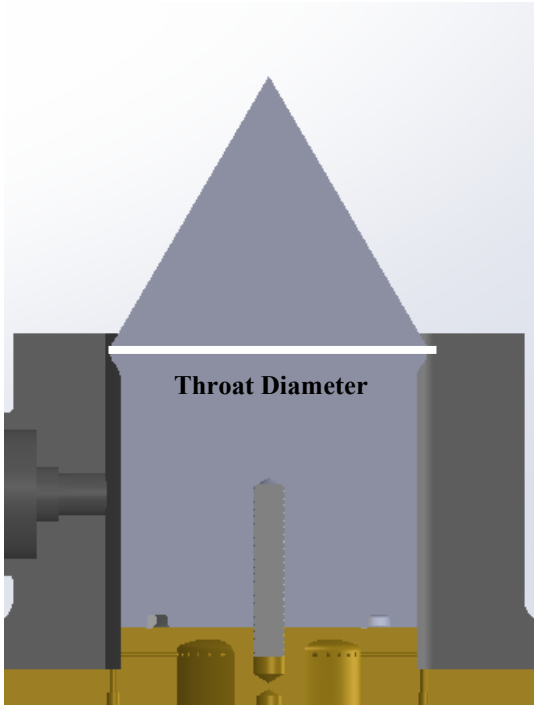

Fig. 6 Cross Section of Inner Body with Throat

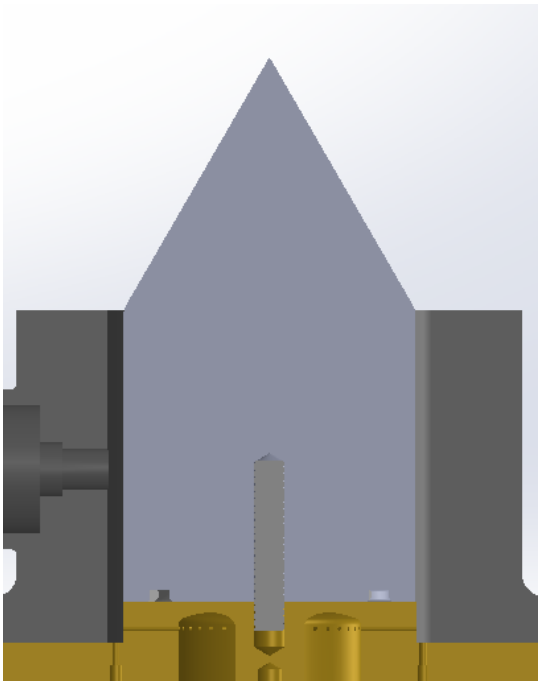

Fig.7 Cross Section of Inner Body without Throat

C. Injector Design

A trade study was performed in which several designs were weighed based on their manufacturability, propellant delivery, mixing efficiency, pressure recovery, design complexity, suitability, and cost effectiveness. This trade study explores three different injector geometries – the doublet impinging, doublet semi-impinging, and doublet jet-in-crossflow. First, functional requirements relevant to the injector were identified, which were then used as a source of derivation for design criteria to evaluate the three options. After consideration of the project's constraints, scoring and weight criteria were developed, and a decision matrix was then made. The three options were qualitatively and quantitatively assessed against the design criteria, and finally evaluated in a decision matrix for selection.

Mixing downstream of Jet in Crossflow (JIC) injector faces is promoted by the vortices that form when the jets of one propellant collide with axial crossflow of the other propellant. The relatively consistent mixing efficiency of JIC geometry have been shown to promote higher chances of achieving detonation. J. Wyatt's thesis on various injector geometries for the Airforce Research Laboratory (AFRL) indicated more consistent detonation across a wider range of equivalence ratios and mass flow rates using JIC injectors compared to pre-mixed JICs and simple spiral geometries [12].

When determining the geometry of the injector components, the team explored several options. The cross section of each option was drawn up and weighed against its opponents. The objective of this design was to minimize the number of components as well as the number of seals required. The machinability of the injector is also large factor and provides a unique challenge due to the tight tolerances and complex geometries required.

Given the small distances between fuel and oxidizer orifices, and the 90-degree orientation of the JIC injector geometry, the orifices must be drilled on separate components to ensure machinability of the injector. The team explored several different two-part and three-part designs. The two-part designs were found to be superior due to the number of seals required, allowing them fewer points of failure compared to the three-part designs. To optimize the area available for fuel orifices, the design makes use of an annular fuel plenum. Note that this plenum features a swept edge above the orifices to impede back flow within the plenum. The fuel and oxidizer manifolds are press-fit together, then fastened

with a single 6-32 countersunk bolt. A dowel pin is used between the fuel and oxidizer manifolds to ensure alignment between each set of orifices. Oxygen is delivered to the oxidizer plenum through three inlets placed radially around the oxygen manifold. This was done to ensure enough clearance for integration with the test stand. The oxygen manifold also features two fuel inlets that carry the fuel from the backing plate to the fuel manifold. The CAD for this design can be found below in Fig. **8** - Fig. .

A major obstacle encountered when designing the injector was determining seal selection and placement. The original design of the injector featured O-rings between the fuel and oxidizer manifolds. This was determined to be ill-favored due to the high cost and lead time associated with ordering custom O-rings small enough for this design. Instead, the team made use of a unique crush seal design that relies on the malleability of brass to compress the components into one another without the use of a seal between. Each injector component features a key-like interface in which one slots into the other before they are crushed together using a hydraulic press. When exposed to the compressive force, the brass of each component will expand into to the other creating a seal like that of a metal crush seal. Once the two components have been compressed and bolted together, it is imperative that they do not be taken apart as the surfaces of each component will be incapable of forming the same seal. A cross section of this design can be found in **Fig.** .

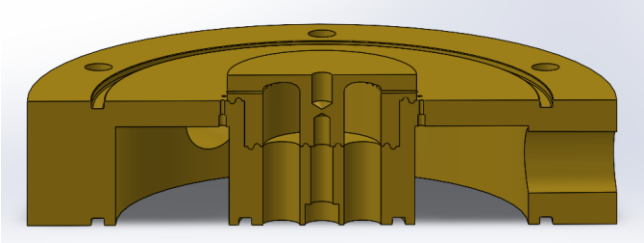

Fig. 8 Cross Section of Injector Assembly

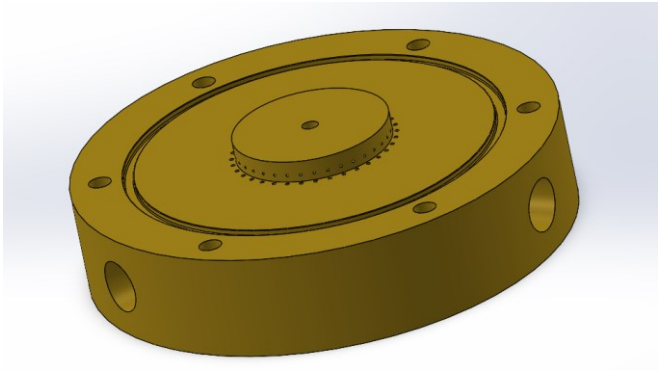

Fig. 9 Full View of Injector Assembly

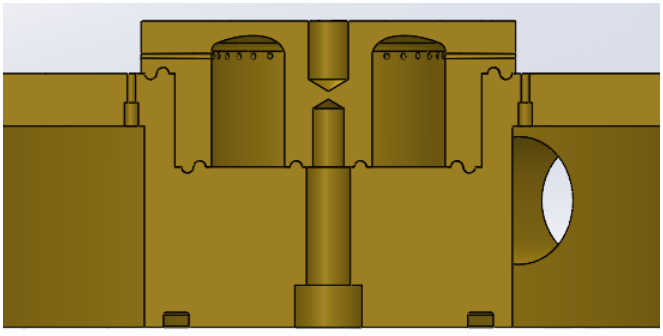

Fig. 10 Cross section of Oxygen to Fuel Manifold Interface

MATLAB was used to size the injection areas for each propellant, as well as to determine a range of operating pressures based on inputs of desired total mass flow rates and equivalence ratios for testing. A combination of simplifying assumptions on specific conditions before and after the orifices were used. The injector was taken to be ideally choked

at the orifices and sharp-edged, implying a Mach number of $M = 1$ and a discharge coefficient (C_d) of 0.65, respectively. Total temperatures of both the gaseous oxygen and methane in the plenums were assumed to be 300 K each. Specific heat ratios (γ) for the propellants were treated as constant.

Specific conditions noted to promote detonation in previously published research were also used to find initial values. Plenum pressure ratio (P_r) and equivalence ratio (φ) were set to match conditions that yielded the most promising results from Burden's experimentation with gaseous methane-oxygen mixtures at near-stoichiometric conditions, specifically at a φ of 1.1, and P_r close to 1 [13,14]. Knowing this, the next step was to identify parameters that can narrow down a total pressure. Fiorino's testing on a 28-mm RDRE showed that total mass flows between 0.05 and 0.075 kg/s exhibited the highest number of detonations at near stoichiometric conditions [15]. Therefore, an initial total mass flow rate of 0.05 kg/s was chosen so that higher plenum pressures would be required to increase mass flow rate, therefore promoting higher static pressures during testing. Finally, Knowlen's experimentation on 25-mm methane-oxygen RDREs required a downstream static pressure for the fresh reactants of at least 540 kPa, as well [16]. A minimum static pressure for the ideal conditions mentioned above was set to be 689.476 kPa, or 100 psi, to expand the range of equivalent ratios, and therefore upstream total pressures, that can be tested and meet the static pressure requirement.

Using the isentropic relationship between static and total pressure in the equation below, a minimum static pressure of 100 psi, a Mach number of $M = 1$, and the respective specific heat ratios of each propellant, the initial total pressure required for each propellant was obtained.

$$P_0 = P\left(1 + \frac{\gamma - 1}{2}M^2\right)^{\frac{\gamma}{\gamma-1}} \tag{2}$$

The larger total pressure of the two propellants was then set as the plenum pressure for both propellants to maintain a P_r of 1 at a φ of 1.1, which was 188.9 psi. Afterwards, the larger total pressure and desired mass flow rate of each propellant derived from the desired φ was incorporated into the equation below to determine the required total injection area for each propellant at the same Mach number.

$$A = \frac{\dot{m}}{C_d P_0}\sqrt{\frac{RT_0}{\gamma}}\left(\frac{1}{M}\left(1 + \frac{\gamma - 1}{2}M^2\right)^{\frac{\gamma+1}{2(\gamma-1)}}\right) \tag{3}$$

Using 36 orifices, the oxygen injector orifice diameter was determined to be 0.032 inches, and the methane injector orifice diameter was determined to be 0.020 inches. Using the determined areas for each propellant, a range of 0.8-1.3 for φ and 0.05-0.1 kg/s for total mass flow rates were inputted in the same injector area equation above, reconfigured for total pressure, to determine a range of operating oxidizer and fuel plenum pressures to test multiple data points. The momentum flux ratio was determined for each data point using the following equation, where variation was only found with changing φ. The ideal condition that the injector was initially sized was determined to have a momentum flux ratio of 0.9607.

$$J = \frac{\gamma_{jet} P_{jet} {M_{jet}}^2}{\gamma_{cross} P_{cross} {M_{cross}}^2} \tag{4}$$

D. Materials and Manufacturability

The materials in this engine were chosen based on constraints of manufacturability and cost. A decision matrix was used to choose the cross examine materials with capabilities and costs. The injector material was chosen as Brass 316, providing adequate strength and thermal capabilities to handle the plenum and channel conditions. Brass is machinable to tight tolerances, allowing for the complex and precise geometry required from the injector to be made. Brass is also ductile enough to allow for the crush seal design, which enabled the injector to be made from two pieces of brass while still ensuring a perfect seal between the fuel plenum and oxidizer plenum. The backplate, not being exposed to any harsh conditions aside from the thrust force of the engine, was made from 304 stainless steel.

The inner body variants and outer body were additively manufactured using Inconel 718. These geometries did not require the precision of the injector and could be 3D printed out of Inconel for a higher strength and thermal capacity. Inconel 718 additive manufacturing is typically used for more complex geometries, however, in terms of the small-scale rotating detonation rocket engine, accessibility to strong materials was limited within the project budget. The unfavorable surface finish from the Direct Metal Laser Sintering (DMLS) technique had to be post-processed through traditional subtractive manufacturing methods. Using an EOS 290m metal 3D printer, the DMLS technique grows the parts on a build platform. Fine Inconel 718 powder roughly, 20 micrometers in diameter, is swept across the previous height and uses a laser to melt and fuse the particles repeatedly at each height. The resulting part is expected to maintain a ±.004" profile tolerance on the exposed features based on the CAD file. When the parts were complete, a wire EDM was used to remove them from the build platform and place them into the machining queue. Due to the material's considerable

hardness and thermal properties, it is not ideal to mainly use subtractive methods with Inconel 718 stock. The local heat generated during a machine pass was not considerable enough to soften the material as it generally would with traditionally machined metals (i.e. 6061 T-6 Aluminum or 304 Stainless Steel). This causes significant wear on the tools during these operations. To avoid the need to purchase extra tooling, the team preferred to slightly overgrow the Inconel 718 parts, additively, and follow up with a finishing subtractive pass to clean up the surfaces and meet the engineering drawing requirements.

I. Analytical Model

A. Description and constraints

As outlined in the previous sections, this RDRE was designed using Bykovskii's constraints[8] and previous data on small-scale RDREs. To ensure reliable operability at the Propulsion and Energy Research Laboratory (PERL) using a gas-gas high pressure blow-down architecture, an analytical model was used. This work uses a modified version of an analytical model that was first introduced by Connolly et. al. and Kiyanda et. al.[4,5]. Their model simplifies the injection area as an isentropic nozzle with a normal shock located at the end of the nozzle. Isentropic flow and shock relations were used to compute the remainder of the state as shown in Figure 11.

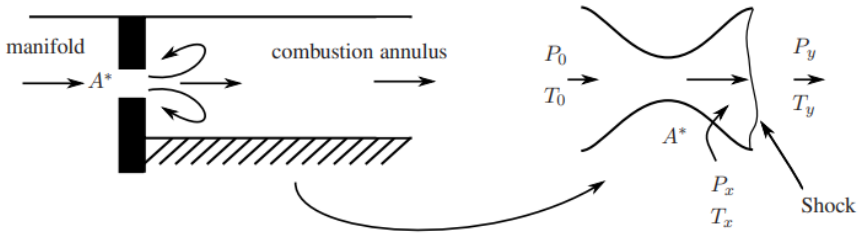

Fig. 11 Isentropic Shock Relations [4,5]

This work explores a different approach to the same analysis. Using the same constraints and assumptions as Connolly et. al. and Kiyanda et. al., the model in this work does not assume premixing and therefore uses different injector areas [4]. By giving the model a desired mass flow and equivalence ratio in the combustion channel, it outputs the required pressures in each manifold using the process outlined in the injector design section. Assuming that the flow exiting the chamber is choked, mass flow in the chamber can be related to the total pressure of the manifolds [17]. The following equations were used to find an effective manifold pressure.

$$P_3^{Eff} = \frac{\sigma_{ox} A_2^{*ox} P_0^{ox} + \sigma_{ox} A_2^{*Fuel} P_0^{Fuel}}{A_3^{Eff} \sigma_{mix}} \tag{5}$$

For any species x:

$$\sigma_x = (\gamma_x + 1)\left(\frac{2}{\gamma_x + 1}\right)^{\frac{\gamma_x}{\gamma_x - 1}} \tag{6}$$

$$A_3^{Eff} = A_2^{*ox} + A_2^{*Fuel} \tag{7}$$

Figure 12 shows a schematic of the cross-section of a test combustor with features that visually represent what is being considered in this study. Location 3 is the mixed pre-shock pressures and location 4 is post shock pressures. The control volume is denoted by a dashed line and the shaded area represents the critical length in which the detonation wave propagates. It is important to note that the combustion channel is choked at the exit in location 5.

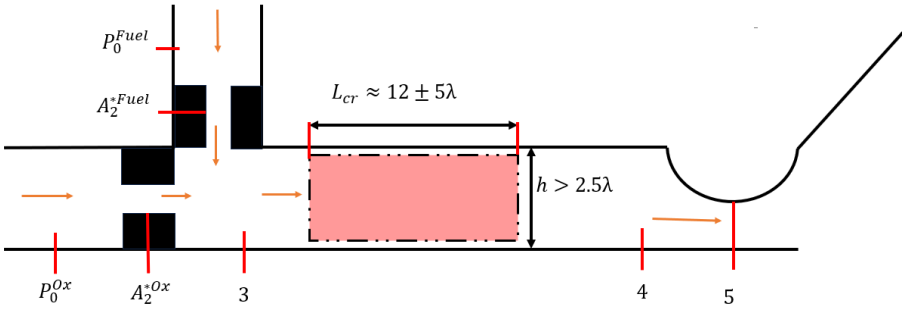

Fig. 12 Test Combustor Cross Section

From the previous assumptions made in this model, the critical length must be several times larger than the annulus height resulting in $L_{cr} > Kh$, where K = 5 represents the scaling factor, the detonation cells within the channel gap can be defined in the following equation. Here, h is channel gap and λ is cell size.

$$\frac{h}{\lambda} \leq 2.4 \pm 1 \tag{8}$$

The inversely proportional relationship of cell size to initial static pressure of unreacted fuel mixture was then used to scale the cell size for every iteration using the following equation [18].

$$P_{ref} = \lambda_{ref} \frac{P_{ref}}{P} \tag{9}$$

Consecutively, the wavenumber (ω) was determined using these same restrictions. Due to the small nature of the RDRE, it assumed that there is only a single detonation cell within the thickness of the channel resulting in a corrected detonation speed of $U_D = U_{CJ} * .6$ [4,5,18]. The U_{CJ} speed is found using NASA CEA. An upper and lower bound is used for every calculation of C_L=17 and C_L=7 respectively to account for the possible variation in critical length.

$$\omega = \frac{\dot{m} R_{sp} T}{C_L \lambda_{ref} P_{ref} U_D h} \geq 1 \tag{10}$$

B. Results

The model receives a range of mass flows at an equivalence ratio and converts them into manifold pressures at the manifold of the propellant manifolds. This data is presented to verify two criteria: (1) The range of wave number needs to lie in a region above ω = 1; (2) Aspect ratio needs to lie within a region above 1.2. This work explores mass flows from .05 kg/s to .1 kg/s at an equivalence ratio of 1.1. Figure 13 shows the change in of aspect ratio values with respect to mass flow rate. The different lines represent gap width. Where the top line is the greatest gap width (h=6mm) and lower line being the lowest gap width (h = 1mm). Figure 14 shows the change of the wave number with respect to mass flow rate. Where the top line is the greatest mass flow ($\dot{m}$=0.1kg/s) and lower line being the lowest mass flow ($\dot{m}$ = 0.05kg/s).

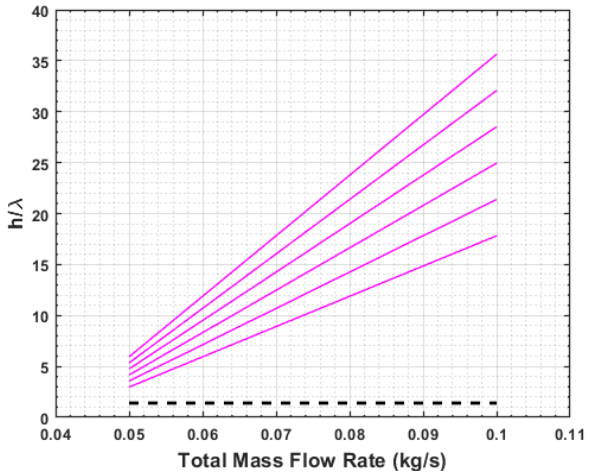

Fig. 13 Cell Width and Initial Pressure

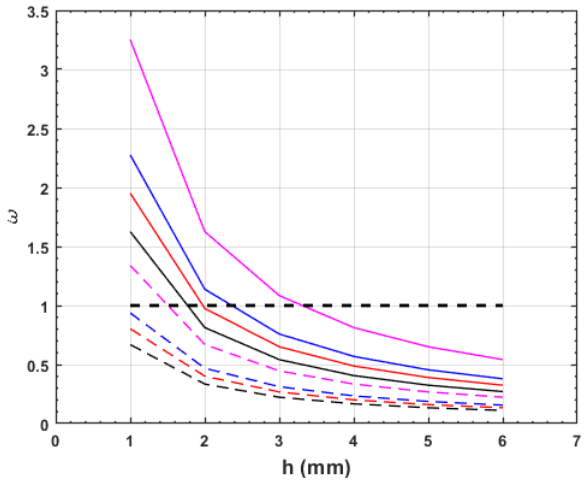

Fig. 14 Wave Number and Varying Gap Width

II. Conclusion

This work explores the complexities that go into designing a Small-Scale Methane/Oxygen Jet-in-Crossflow Rotating Detonation Engine. Using the framework provided by Bykovskii's constraints [8] and a mathematical model for small-scale RDRE's [4,5], the team successfully designed a RDRE with criteria to achieve one detonation wave minimum based on fundamental isentropic relations. Using the data collected, a testing campaign will be developed to experientially test the hardware at the Propulsion and Energy Research Laboratory.

III. Acknowledgements

This work would not be possible without the incredible mentorship from Dr. Robert Burke, David Scott Hanon, Adam Kotler, Dr. Kurt Stresau and Dr. Kareem Ahmed. The authors would also like to acknowledge the University of Central Florida- Mechanical and Engineering department, Propulsion and Energy Research Laboratory (PERL) and Knights Experimental Rocketry group for their sponsorship in this project.

IV. References

[1] Roberts, Q., and Knowlen, C., "Pre-Ignition Propellant Mixing in Small Scale Rotating Detonation Rocket Engines," 2024. https://doi.org/10.2514/6.2024-2034

[2] Knowlen, C., Mundt, T. J., Roberts, Q., Hamza, A., Menn, D., and Kurosaka, M., "Operating Characteristics of a 10-Mm Rotating Detonation Rocket Engine," 2024. https://doi.org/10.2514/6.2024-2610

[3] Pennington, J. C., Gray, J. A., Sell, B. C., Schauer, F., Polanka, M. D., and Feleo, A., "Study of the Performance Characteristics of a Micro Rotating Detonation Engine Using a Stewart Platform," 2024. https://doi.org/10.2514/6.2024-0812

[4] Connolly-Boutin, S., Joseph, V., Ng, H. D., and Kiyanda, C. B., "Small-Size Rotating Detonation Engine: Scaling and Minimum Mass Flow Rate," *Shock Waves*, Vol. 31, No. 7, 2021, pp. 665–674. https://doi.org/10.1007/s00193-021-00991-2

[5] Kiyanda, C. B., Connolly-Boutin, S., Joseph, V., Mi, X., Ng, H. D., and Higgins, A. J., "Small Size Rotating Detonation Engine: Scaling and Minimum Mass Flow Rate."

[6] Mundt, T., "Geometric Scaling of Cylindrical Rotating Detonation Rocket Engine Combustors."

[7] Knowlen, C., Mundt, T. J., and Kurosaka, M., "Experimental Results for Geometrically Scaled Rotating Detonation Rocket Engines," 2023. https://doi.org/10.2514/6.2023-0354

[8] Bykovskii, F. A., Zhdan, S. A., and Vedernikov, E. F., "Continuous Spin Detonations," *Journal of Propulsion and Power*, Vol. 22, No. 6, 2006, pp. 1204–1216. https://doi.org/10.2514/1.17656

[9] Kaneshige, M., and Shepherd, J. E., "Detonation Database," 1997.

[10] Schumaker, S. A., Knisely, A. M., Hoke, J. L., and Rein, K. D., "Methane–Oxygen Detonation Characteristics at Elevated Pre-Detonation Pressures," *Proceedings of the Combustion Institute*, Vol. 38, No. 3, 2021, pp. 3623–3632. https://doi.org/10.1016/j.proci.2020.07.066

[11] Goto, K., Nishimura, J., Kawasaki, A., Matsuoka, K., Kasahara, J., Matsuo, A., Funaki, I., Nakata, D., Uchiumi, M., and Higashino, K., "Propulsive Performance and Heating Environment of Rotating Detonation Engine with Various Nozzles," *Journal of Propulsion and Power*, Vol. 35, No. 1, 2019, pp. 213–223. https://doi.org/10.2514/1.B37196

[12] J. Wyatt, J., "Injection Studies on a Small-Scale Rotating Detonation Engine with Improved Flow Control AIR FORCE INSTITUTE OF TECHNOLOGY," 2021.

[13] Burden, A., Burke, R., Kotler, A., Rezzag, T., Schuetz, S., and Ahmed, K., "Experimental Investigation of Injector Sizing In The Rotating Detonation Rocket Engine," 2022. https://doi.org/10.2514/6.2022-4106

[14] Burden, A. M., Burke, R. F., Rezzag, T., Jacobson, J., Schuetz, S., and Ahmed, K. A., "Characterization of Injection Mixing in The Rotating Detonation Rocket Engine," 2023. https://doi.org/10.2514/6.2023-0572

[15] Fiorino, N. T., Snow, N. J., Schauer, F. R., Polanka, M. D., Alexander Schumaker, S., and Sell, B. C., "Improving Detonability in a Small-Scale Rotating Detonation Engine Using Partial Premixing," *Journal of Propulsion and Power*, 2022, pp. 1–10. https://doi.org/10.2514/1.B38668

[16] Knowlen, C., Mundt, T., and Kurosaka, M., "Experimental Results for 25-Mm and 51-Mm Rotating Detonation Rocket Engine Combustors," *Shock Waves*, Vol. 33, No. 3, 2023, pp. 237–252. https://doi.org/10.1007/s00193-023-01120-x

[17] Bach, E., Thethy, B. S., Edgington-Mitchell, D., Haghdoost, M. R., Paschereit, C. O., Stathopoulos, P., and Bohon, M. D., "Kiel Probes for Stagnation Pressure Measurement in Rotating Detonation Combustors," *AIAA Journal*, Vol. 60, No. 6, 2022, pp. 3724–3735. https://doi.org/10.2514/1.J061061

[18] B. V. Voitsekhovskii, "The Spin Detonation," *Dokl. Akad. Nauk SSSR*, 1957.